Universal low-frequency asymptotes of dynamic conic nanopore rectification: An ionic nanofluidic inductor

Yu Yan, Jarrod Schiffbauer, Gilad Yossifon, and Hsueh-Chia Chang

Citation: The Journal of Chemical Physics **143**, 224705 (2015); doi: 10.1063/1.4937360
View online: http://dx.doi.org/10.1063/1.4937360
View Table of Contents: http://scitation.aip.org/content/aip/journal/jcp/143/22?ver=pdfcov
Published by the AIP Publishing

Universal low-frequency asymptotes of dynamic conic nanopore rectification: An ionic nanofluidic inductor

Yu Yan,[1] Jarrod Schiffbauer,[2] Gilad Yossifon,[2] and Hsueh-Chia Chang[1,a)]
[1]*Department of Chemical and Biomolecular Engineering, University of Notre Dame, Notre Dame, Indiana 46556, USA*
[2]*Micro- and Nanofluidics Laboratory, Faculty of Mechanical Engineering, Technion-Israel Institute of Technology, Technion City 32000, Israel*

(Received 30 September 2015; accepted 24 November 2015; published online 10 December 2015)

We report the first nanofluidic inductor (L) to complement the known nanofluidic capacitors (C), resistors (R), and diodes for ion currents. Under negative bias, the nanopore behaves like a parallel RC circuit at low frequencies; however, under positive bias, the asymptotic dynamics is that of a serial RL circuit. This new ionic circuit element can lead to nanofluidic RLC or diode-inductor oscillator circuits and new intrapore biosensing/rapid sequencing strategies. A universal theory, with explicit estimates for the capacitance and inductance at opposite biases, is derived to collapse the rectified dynamics of all conic nanopores to facilitate design of this new nanofluidic circuit. © *2015 AIP Publishing LLC.* [http://dx.doi.org/10.1063/1.4937360]

There are many anticipated applications for nanofluidic circuits that can mimic semiconductor (and neuron) circuitry to produce oscillations, hysteresis, and excitability.[1] Field and current focusing into nanochannels lead to natural ionic resistors.[2] Double-layer ionic capacitors have led to super-capacitor batteries.[3] Ionic rectifiers have been constructed from nanopores with asymmetric charge distributions or geometry.[4] However, an ionic inductor has never been reported, thus preventing the creation of nanofluidic circuits like the RLC oscillator and the diode-inductor Chua circuits.[5] We report such an ionic inductor here and offer a universal theory for its inductance based on non-equilibrium nanofluidic ion transport dynamics within a conic nanopore.

Because the inductor dynamics is caused by intrapore ion transport, this ionic element also suggests new nanopore biosensing and rapid sequencing applications. Electrical Impedance Spectroscopy (EIS),[6] probing the Warburg spectrum in particular, with universal Warburg phase lag due to external transport limitation of charged molecules, is a standard biosensing technique.[7] Ion current dynamics due to intrapore charge molecule transport may extend the technique to the detection of a single molecule in a nanochannel/nanopore[8] and identification of its sequence.[9]

We construct such a nanofluidic inductor from the DC conic nanopore diode. The DC rectification is due to internal ion depletion/enrichment because of discontinuous ionic fluxes that arise from conductivity gradients imposed by the converging pore.[10] This non-uniform ion concentration profile can also be generated by the AC voltage. Coupled with DC field, it can produce an oscillating ion current that either leads or lags the voltage oscillation, corresponding to capacitive or inductive dynamics. A universal theory is developed for all conic pores by an asymptotic expansion.

We first experimentally demonstrate the AC impedance features due to intrapore ion enrichment and depletion in conic nanopores. The experiments are carried out by Gamry Reference 600 in a negatively charged silica conic nanopipette pulled by P-2000 Sutter Instrument.[11] Symmetric electrolyte KCl and Ag/AgCl electrodes are used. A typical Nyquist plot for the complex impedance function $Z(\omega)$ is shown in Fig. 1. For forward (positive) bias (electric field is applied from the tip to base), with a lower DC impedance due to intrapore enrichment, the impedance spectrum spirals towards the real axis like a RCL circuit at low frequencies, with a significant portion exhibiting a phase lag. Although the conic nanopore spectrum will be shown to be universal for all frequencies, the higher-frequency portion will be camouflaged by the usual double-layer RC dynamics and only the low-frequency portion close to the real-line will be collapsed by the theory. For negative bias, with a larger DC impedance due to intrapore depletion, the curvature of the low-frequency impedance spectrum changes sign and converges to the real line in a semi-circle like a parallel RC circuit. The positive lead is reminiscent of the classical Randall RC circuit without the distinct inductance feature with phase lag for positive bias. Since the AC impedance measures the change in resistance due to the AC forcing, the zero-frequency asymptotes of both spectra do not approach the DC impedance value with the same bias, as shown in Fig. 1, but to a universal asymptote value for both biases, as will be shown below.

We begin by deriving the dynamic conductance for the conic nanopore under an AC field with a DC bias. For slender cones, the radial and angular components are separable for both the concentration and electric fields. We shall examine the small X_{tip} region in the phase diagram (Fig. 5) of Yan *et al.*[10] where intra-pore concentration polarization occurs and is responsible for current rectification. In this region, the tip radius is significantly larger than the Debye length and the charge spill-over phenomenon described by Sherwood

a)Author to whom correspondence should be addressed. Electronic mail: hchang@nd.edu

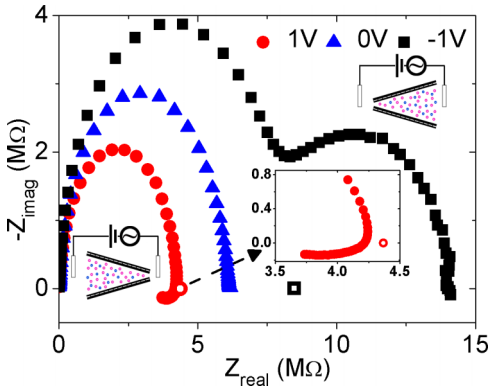

FIG. 1. A Nyquist plot showing voltage dependent impedance for a conic nanopipette at different DC bias. A nanopipette with a DC rectification factor of 1.9 for 1M KCl solution at +1 V/−1 V is used. The forward bias is from the tip to base. At low frequency, the forward bias has an inductive response, while the backward has a capacitive response. Both sets of impedance spectra do not approach the DC value shown as open symbols in the figure, giving rise to a finite AC impedance contribution at zero frequency.

et al.[12] does not occur. Hence, an electroneutral condition can be imposed. After cross-sectional averaging in the angular coordinate, using operator[10,13] $\langle\rangle = \frac{1}{1-\cos\theta_m}\int_0^{\theta_m} d\theta \sin\theta$ (θ_m is the half-cone angle), the Poisson equation yields to leading order the local (longitudinal) electroneutrality condition to leading order,

$$zF(\langle C_+\rangle - \langle C_-\rangle) = \frac{2\sigma_s}{R_p}, \tag{1}$$

provided that the Debye length is much smaller than pore length, where σ_s is the amount of negative surface charge, R_p is local radius, $C_\pm$ are the concentration of cation and anion, z is the valency, and F is Faraday constant. This local neutrality produces local mobile ion concentrations that are functions of the local pore radius R_p and a corresponding potential related to this concentration. A conic nanopore without surface charge would have an intrapore ion concentration equal to the bulk, a focused field, and a flux due to pure electro-migration—it is at equilibrium with the bulk. In contrast, a charged conic pore with a varying radius would have an excess longitudinal concentration gradient to produce additional electro-migration and diffusion fluxes. Any point within the charged conic pore is not at equilibrium with the bulk but is instead constrained by the electro-neutrality condition (Eq. (1)).

We demonstrate this mechanism by cross-sectional averaging the Nernst-Planck equations for the total ion and current flux in the longitudinal r direction. It produces the following equations for the ion concentration and electrical field (see Ref. 10 for details):

$$\frac{\partial\langle C\rangle}{\partial t} = \frac{1}{r^2}\frac{\partial}{\partial r}r^2\left(\frac{\partial\langle C\rangle}{\partial r} + \frac{\varepsilon}{r}\frac{\partial\phi}{\partial r}\right), \tag{2a}$$

$$0 = \frac{1}{r^2}\frac{\partial}{\partial r}r^2\left(-\frac{\varepsilon}{r^2} + \langle C\rangle\frac{\partial\phi}{\partial r}\right), \tag{2b}$$

where $\langle C\rangle = \langle C_+\rangle + \langle C_-\rangle$, and the averaged charged density $\langle C_+\rangle - \langle C_-\rangle$ is replaced by the electroneutrality condition (Eq. (1)). The total concentration is allowed to vary in time but there is no charge accumulation. The characteristic scaling properties are the pore length $L = (R_{base} - R_{tip})/\theta_m$, the bulk concentration C_0, the diffusion time L^2/D, the current $2\pi FZ(1-\cos\theta_m)DC_0L$, and the thermal potential RT/zF. With this scaling, the tip and base are located at $r_1 = \frac{R_{tip}}{R_{base}-R_{tip}}$ and $r_2 = \frac{R_{base}}{R_{base}-R_{tip}}$, such that $r_2 = r_1 + 1$. The parameter $\varepsilon = \frac{\sigma_s\sin\theta_m}{zFC_0L(1-\cos\theta_m)}$ represents the dimensionless surface charge scaled by the bulk concentration. The two locations that appear in Eqs. (2a) and (2b) represent the excess respective electromigration and diffusive fluxes due to the mobile ion concentration variation stipulated by the electroneutrality condition (Eq. (1)).

The tip and base are in equilibrium with the bulk, hence the applied voltage (both the DC bias and the AC forcing at the tip) is added to the Donnan equilibrium potential based on the tip and base ionic strengths.[10] The 4 relevant boundary conditions are hence the dimensionless potential and total ion concentration at each boundary, indicated by subscripts 1 and 2: $\phi_1 = V_0 + \delta\sin(w_0t) - \ln(X_1/2 + \sqrt{(X_1/2)^2+1})$, $\phi_2 = -\ln(X_2/2 + \sqrt{(X_2/2)^2+1})$, and $\langle C\rangle_{1,2} = \sqrt{X_{1,2}^2+4}$, where δ and w_0 are the dimensionless AC amplitude and frequency ($\omega_0 = \omega L^2/D$, ω is dimensional frequency) and $X = \frac{2\sigma_S}{zFC_0R_p}$ (for small cone angle, $X = \frac{\varepsilon}{r}$) is the effective surface charge concentration at either $R_p = R_{tip}$ ($r = r_1$) or $R_p = R_{base}$ ($r = r_2$). There are hence four system parameters for the problem: ε, δ, ω_0, plus the nanopore geometry parameter r_1. However, with proper expansion in the first two parameters, we will demonstrate a universal scaling that is only a function of the geometry parameter r_1 and the frequency ω_0. Another expansion offers a universal expression with a universal number for the zero-frequency AC impedance, seen in Fig. 1.

For a weakly selective nanopore ($X \sim \varepsilon \ll 1$), two small parameters are present, ion selectivity ε and perturbation voltage, δ (assumed small compared to the applied DC bias). We extract their scaling explicitly with a simple ansatz expansion for weak charge and small AC forcing, $\langle C\rangle = \langle C\rangle_0 + \varepsilon\langle C\rangle_\varepsilon + \varepsilon^2\langle C\rangle_{\varepsilon^2} + \delta\langle C\rangle_\delta + \varepsilon\delta\langle C\rangle_{\varepsilon\delta}\cdots$. The DC $O(1)$ order solution (without surface charge) and the $O(\varepsilon)$ order solution (with surface charge) are the same as our previous theory:[10] $\langle C\rangle_0 = 2$, $\phi_0 = \frac{V_0r_1(r_2-r)}{r}$ with $I_0 = 2r_1r_2V_0$ and $\langle C\rangle_\varepsilon = \frac{V_0(r_2-r)(r-r_1)}{2r^2}$ with $I_\varepsilon = \frac{V_0^2}{12}$. The two currents I represent the symmetric (unrectified) value due to conic focusing without surface charge and the rectifying correction due to surface charge. The $O(\varepsilon)$ current correction $\varepsilon I_\varepsilon = \varepsilon V_0^2/12$ describes enrichment/depletion for forward/backward bias, the key intrapore rectification mechanism, and offers a universal scaling that collapses simulated and experimental DC data.[10]

The $O(\varepsilon^2)$ is not a dynamic order and it does not contribute to the AC impedance. The same is true for $O(\varepsilon^3)$, $O(\varepsilon^4)$, and so on. They are not solved here.

The first non-trivial dynamic order $O(\delta)$ is $i\omega_0\langle\tilde{C}\rangle_\delta = \frac{1}{r^2}\frac{d}{dr}r^2(\frac{d\langle\tilde{C}\rangle_\delta}{dr})$ and $0 = \frac{1}{r^2}\frac{d}{dr}r^2(\langle C\rangle_0\frac{d\tilde{\phi}_\delta}{dr} + \langle\tilde{C}\rangle_\delta\frac{d\phi_0}{dr})$ after transformation $\langle C\rangle_\delta = Im(\langle\tilde{C}\rangle_\delta e^{i\omega_0t})$ and $\phi_\delta = Im(\tilde{\phi}_\delta e^{i\omega_0t})$, where $\langle\tilde{C}\rangle_\delta$ and $\tilde{\phi}_\delta$ are complex functions dependent only upon r_1 and w_0. This order, however, produces no concentration correction and simply a quasi-steady current correction $\langle\tilde{C}\rangle_\delta = 0$, $\tilde{\phi}_\delta = \frac{r_1(r_2-r)}{r}$, and $\tilde{I}_\delta = 2r_1r_2$.

The distinct phase lags occur at the cross-order $O(\varepsilon\delta)$, after the same transformation as before,

$$i\omega_0\langle\tilde{C}\rangle_{\varepsilon\delta} = \frac{1}{r^2}\frac{d}{dr}r^2\left(\frac{d\langle\tilde{C}\rangle_{\varepsilon\delta}}{dr} + \frac{1}{r}\frac{d\tilde{\phi}_\delta}{dr}\right), \tag{3a}$$

$$0 = \frac{1}{r^2}\frac{d}{dr}r^2\left(\langle\tilde{C}\rangle_{\varepsilon\delta}\frac{d\phi_0}{dr} + \langle C\rangle_0\frac{d\tilde{\phi}_{\varepsilon\delta}}{dr} + \langle\tilde{C}\rangle_\delta\frac{d\phi_\varepsilon}{dr} + \langle C\rangle_\varepsilon\frac{d\tilde{\phi}_\delta}{dr}\right), \tag{3b}$$

with trivial boundary conditions. From Eq. (3b), the current $I_{\varepsilon\delta}$ satisfies: $\int_{r_1}^{r_2} -\frac{\tilde{I}_{\varepsilon\delta}}{r^2}dr = \int_{r_1}^{r_2}\left(\langle\tilde{C}\rangle_{\varepsilon\delta}\frac{d\phi_0}{dr} + \langle C\rangle_\varepsilon\frac{d\tilde{\phi}_\delta}{dr}\right)dr$ after getting rid of trivial terms. The first term is from the perturbation concentration due to AC voltage (Eq. (3b)) under DC bias, while the second is from the concentration due to DC bias under AC voltage.

Eq. (3a), combined with the $O(\delta)$ electric field, yields $i\omega_0\langle\tilde{C}\rangle_{\varepsilon\delta} = \frac{1}{r^2}\frac{d}{dr}r^2\left(\frac{d\langle\tilde{C}\rangle_{\varepsilon\delta}}{dr} - \frac{r_1r_2}{r^3}\right)$, which does not depend on the DC bias at all. After transformation[14] $H = r^{1/2}\langle\tilde{C}\rangle_{\varepsilon\delta}$ and $x = (-i\omega_0)^{1/2}r$, it becomes $x^2\frac{d^2H}{dx^2} + x\frac{dH}{dx} + (x^2 - 1/4)H = -\frac{(-i\omega_0)^{3/4}r_1r_2}{x^{3/2}}$. This is a Bessel equation of 1/2 order. A particular solution can be achieved through integration[14] $H_p = -(-i\omega_0)^{3/4}r_1r_2J_{1/2}(x)\int\frac{1}{J_{1/2}^2(x)x}\left(\int x^{-5/2}J_{1/2}(x)dx\right)dx$. Hence, the coefficient of the solution

$$H = AJ_{1/2}(x) + BY_{1/2}(x) + H_p(x) \tag{4}$$

can be evaluated by the two homogeneous concentration boundary conditions at this order, $H(x_1) = H(x_2) = 0$,

$$A = \frac{Y_{1/2}(x_2)H_p(x_1) - H_p(x_2)Y_{1/2}(x_1)}{Y_{1/2}(x_1)J_{1/2}(x_2) - Y_{1/2}(x_2)J_{1/2}(x_1)},$$

$$B = \frac{H_p(x_2)J_{1/2}(x_1) - J_{1/2}(x_2)H_p(x_1)}{Y_{1/2}(x_1)J_{1/2}(x_2) - Y_{1/2}(x_2)J_{1/2}(x_1)}.$$

The complex functions H_p and $\langle\tilde{C}\rangle_{\varepsilon\delta}$ are the only functions of the geometric parameter r_1 and the frequency ω_0. Fig. 2 shows the AC perturbed concentration profile $\langle C\rangle_{\varepsilon\delta} = Im(\langle\tilde{C}\rangle_{\varepsilon\delta}e^{i\omega_0 t})$ along the nanopore for various phase angles $\omega_0 t$. In the numerical simulation, the DC steady state solution is used as an initial condition for the simulation (1D average full Poisson-Nernst-Planck equations). All the curves are taken at a sufficiently long time so that the initial condition no longer has an effect on the result. The AC perturbed concentration profile is achieved by subtracting the DC profile from the simulated AC profile and then dividing by $\epsilon\delta$. It is shown in Fig. 2 that the simulation agrees well with the analytical solution evaluated from Eq. (4). The perturbed concentration due to the AC voltage is independent of DC bias and not in phase with the AC signal—the phase at every location is actually different at the same instant in time.

Although the AC perturbed concentration does not depend on the polarization of the DC bias, its contribution to the current, through coupling with DC electrical field, is opposite for different polarities. Hence, there is a π phase angle difference for its current contribution. That is why one direction has a positive phase angle, while the other has a negative phase angle.

The ansatz allows us to isolate the complex conductance, i.e., the inverse AC impedance, $1/Z(\omega_0)$, of the conic nanopore $\tilde{G} = (\delta\tilde{I}_\delta e^{i\omega_0 t} + \varepsilon\delta\tilde{I}_{\varepsilon\delta}e^{i\omega_0 t})/\delta e^{i\omega_0 t} = \tilde{I}_\delta + \varepsilon\tilde{I}_{\varepsilon\delta} = 2r_1r_2 + \varepsilon V_0/12 + \varepsilon r_1^2r_2^2V_0\int_{r_1}^{r_2}\left(\frac{\langle\tilde{C}\rangle_{\varepsilon\delta}}{r^2}\right)dr$. Here, the last term is due to the AC perturbed concentration, such that

$$\frac{\tilde{G} - 2r_1r_2}{\varepsilon V_0} - 1/12 = \tilde{f} = r_1^2r_2^2\int_{r_1}^{r_2}\left(\frac{\langle\tilde{C}\rangle_{\varepsilon\delta}}{r^2}\right)dr \tag{5}$$

where the universal function $\tilde{f}$ is only a function of r_1 (with $r_2 = r_1 + 1$) and the frequency ω_0. The AC conductance is related to this function by $\varepsilon V_0\tilde{f}$. In Fig. 3, the complex function $\tilde{f}$ for a given r_1 is shown as a function of frequency ω_0. Two limits of this universal function can be derived explicitly. At high frequency, the concentration relaxation cannot keep up with the AC bias, hence $\langle\tilde{C}\rangle_{\varepsilon\delta} = 0$. Thus, the conductance is the same as the DC conductance. At low frequency limit, the concentration relaxation is instantaneous and hence in phase, $\langle\tilde{C}\rangle_{\varepsilon\delta} = \frac{(r_2-r)(r-r_1)}{2r^2}$ (similar to $O(\varepsilon)$ order, since it is completely in phase) and $\tilde{G} = G_{diff} = 2r_1r_2 + \varepsilon V_0/6$.

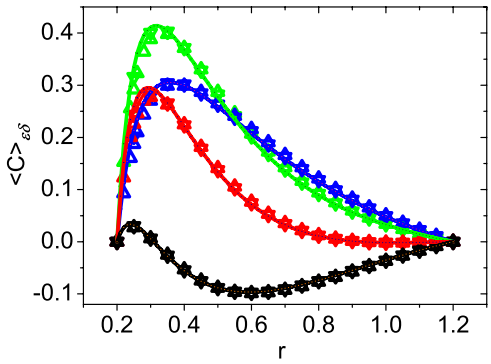

FIG. 2. Comparison of the numerical solution (line) and analytical solution (symbol) AC-perturbed concentration profiles along the conic nanopore for various phases (black: $\pi/8$, red: $3\pi/8$, green: $5\pi/8$, and blue: $7\pi/8$). The nanopore parameters are tip radius 50 nm, base radius 300 nm, length 12 μm, surface charge 0.05 C/m^2, and concentration 1M KCl. The dimensionless DC bias are 40 (~1 V up triangle) and −40 (~−1 V down triangle). The AC frequency and dimensionless amplitude are 25 Hz and 1, respectively.

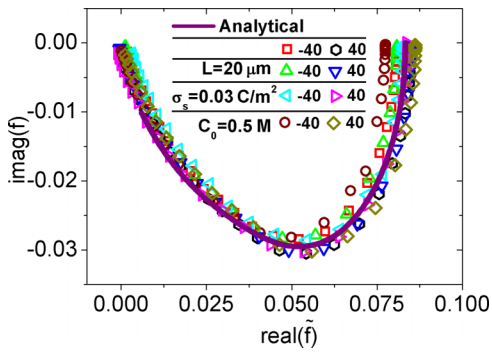

FIG. 3. Collapse of 1D numerical simulation data with Eq. (5) for fixed $r_1 = 0.2$ (and $r_2 = 1.2$), corresponding to a tip radius of 50 nm and a base radius of 300 nm. Frequency increases from right to left with the zero frequency limit at $\tilde{f} = 1/12$. The dimensionless DC bias is 40/−40 (~1 V/−1 V) as indicated and the dimensionless AC amplitude δ is 1. The length, bulk concentration, and surface charge are 12 μm, 1M, 0.05 C/m^2 unless specified otherwise.

This conductance, in fact, is the differential conductance at DC voltage V_0.

This universal zero-frequency limit corresponds to the universal number $\tilde{f} = 1/12$ in Fig. 3 and corresponds to the universal non-zero AC contribution to the zero-frequency impedance seen in Fig. 1.

For frequency approaching to zero frequency, Fig. 3 shows the real part of $\tilde{f}$ remains constant but its imaginary part grows linearly with increasing frequency. In fact, another expansion of $\langle\tilde{C}\rangle_{\varepsilon\delta}$ (Eq. (3a)), with ω_0 as a small parameter, generates $\langle\tilde{C}\rangle_{\varepsilon\delta} = \frac{(r_2-r)(r-r_1)}{2r^2} + i\omega_0((-r^2/6 + (r_1 + r_2)r/2 - r_1r_2lnr)/2 + A' + B'/r) + O(\omega_0^2)$, where A' and B' are the constants determined by boundary conditions $\langle\tilde{C}\rangle_{\varepsilon\delta}\big|_{r_1,r_2} = 0$. Combined with Eq. (5), it gives rise to $\tilde{G} = G_{diff} - i\omega_0\varepsilon V_0 h$, where $h = r_1^2r_2^2 - (r_1 + r_2)r_1^2r_2^2ln(r_2/r_1)/2 + r_1r_2/12$ is only a function of r_1 ($r_2 = r_1 + 1$, $r_1 > 0$) and always has a positive value. For positive bias and small ω_0, the complex impedance $1/\tilde{G} = 1/(G_{diff} - i\omega_0\varepsilon V_0 h) \sim 1/G_{diff} + i\omega_0 L_p$. This is a serial RL circuit with differential resistance $1/G_{diff}$ at V_0 as the resistance and an inductance of $L_p = \varepsilon V_0 h/G_{diff}^2$. For negative bias, the complex conductance $\tilde{G} = G_{diff} + i\omega_0 C_p$, it is a RC parallel circuit with differential resistance at V_0 as the resistance and a capacitor $C_p = \varepsilon|V_0|h$.

This then explains the phase lags in the impedance spectra of Fig. 1. A change from positive to negative phase angles with decreasing modulus, as frequency decreases, leads to the spiral like structure for positive bias. Increase in phase angle produces a curvature change for negative bias.

The above theory for nanopore conductance neglects external resistance and capacitance. To quantitatively capture the full impedance spectra of Fig. 1, we augment it with a bulk resistor R_1, accounting for both field focusing and bulk resistance, and a Debye double-layer capacitor C_1 in the Randall-like circuit[15] of Fig. 4. Both R_1 and C_1 are fitted by the high frequency part of the impedance curve and kept as constants for different bias. From the fitting, $R_1 = 76$ kΩ, which is very close to the access resistance due to field focusing into the nanopore $R_{access} = \frac{RT}{8z^2F^2DC_0R_{tip}} = 62$ kΩ.[10,16] The bottom inset of Fig. 4 shows the analytical spectra for the given parameters. The actual nanopore length is about around 1 cm. Here, we use a cutoff length 44.72 μm since the rest contributes less than 5% to the resistance for better numerical convergence of evaluation of Eq. (5). The experiment spectra are in quantitative agreement with the simple analytical expression offered by the Randall circuit with the low frequency complex nanopore conductance given by Eq. (5) which captures the universal scaling for the intrapore enrichment and depletion dynamics responsible for the asymmetric inductance and capacitance behavior at opposite biases, as well as the universal low-frequency scaling that includes the zero-frequency AC conductance correction $\varepsilon V_0/12$.

The complex impedance model for the conic nanopore, $Z = R_1 + 1/[i\omega C_1 + \frac{2\pi F^2z^2(1-cos\theta_m)DC_0L}{RT}(2r_1r_2 + \varepsilon V_0(\frac{1}{12} + \tilde{f}))]$, with the low frequency capacitor and inductor asymptote ($L_p = \varepsilon V_0 h/G_{diff}^2$ for positive bias and $C_p = \varepsilon|V_0|h$ for negative bias), should allow the deconvolution of EIS signals to isolate intrapore dynamics relevant to biosensing[7,8] and rapid sequencing.[9]

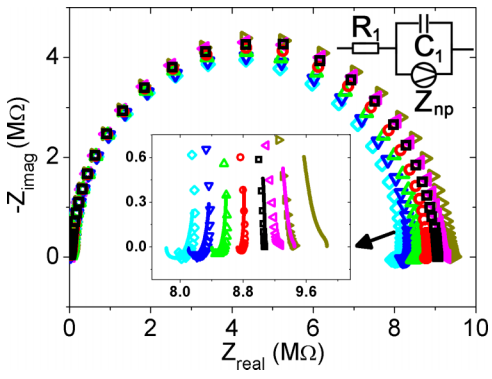

FIG. 4. Experimental data for conic nanopore at different DC bias voltage (0 V black square, 0.5 V red circle, 1 V green up triangle, 1.5 V blue down triangle, 2 V cyan diamond, −0.5 V magenta left triangle, and −1 V dark yellow right triangle) in 1M KCl solution. The bottom inset is the analytical solution (line, same color as symbol) with the following parameters: tip radius 53 nm, half-cone angle 2.5°, cutoff length 44.72 μm, surface charge 0.065 C/m^2, $R_1 = 76$ kΩ, and $C_1 = 9.08$ pF. The right inset is the equivalent circuit of conic nanopore.

Y.Y. and H.C.C. are supported by NSF No. CBET1065652. G.Y. and H.C.C. are supported by US-Israel Binational Science Foundation (BSF) Grant No. 2009371.

[1]D. B. Strukov, G. S. Snider, D. R. Stewart, and R. S. Williams, Nature **453**, 80 (2008); A. Thomas, J. Phys. D: Appl. Phys. **46**, 093001 (2013).
[2]D. Stein, M. Kruithof, and C. Dekker, Phys. Rev. Lett. **93**, 035901 (2004).
[3]P. Simon and Y. Gogotsi, Nat. Mater. **7**, 845 (2008).
[4]Z. Siwy and A. Fuliński, Phys. Rev. Lett. **89**, 198103 (2002); C. Wei, A. J. Bard, and S. W. Feldberg, Anal. Chem. **69**, 4627 (1997); Z. Siwy, E. Heins, C. C. Harrell, P. Kohli, and C. R. Martin, J. Am. Chem. Soc. **126**, 10850 (2004); G. Yossifon, Y.-C. Chang, and H.-C. Chang, Phys. Rev. Lett. **103**, 154502 (2009).
[5]L. Chua, IEEE Trans. Circuits Syst. **27**, 1059 (1980); T. Matsumoto, *ibid.* **31**, 1055 (1984).
[6]D. D. Macdonald, Electrochim. Acta **51**, 1376 (2006); J. Schiffbauer and G. Yossifon, Phys. Rev. E **86**, 056309 (2012); J. Schiffbauer, S. Park, and G. Yossifon, Phys. Rev. Lett. **110**, 204504 (2013).
[7]J. S. Daniels and N. Pourmand, Electroanalysis **19**, 1239 (2007); H.-C. Chang and G. Yossifon, Biomicrofluidics **3**, 012001 (2009); S. Basuray, S. Senapati, A. Aijian, A. R. Mahon, and H.-C. Chang, ACS Nano **3**, 1823 (2009).
[8]S. Das, P. Dubsky, A. van den Berg, and J. C. T. Eijkel, Phys. Rev. Lett. **108**, 138101 (2012); M. Mihovilovic, N. Hagerty, and D. Stein, *ibid.* **110**, 028102 (2013).
[9]D. Branton, D. W. Deamer, A. Marziali, H. Bayley, S. A. Benner, T. Butler, M. Di Ventra, S. Garaj, A. Hibbs, X. Huang *et al.*, Nat. Biotechnol. **26**, 1146 (2008).
[10]Y. Yan, L. Wang, J. Xue, and H.-C. Chang, J. Chem. Phys. **138**, 044706 (2013).
[11]Y. Fu, H. Tokuhisa, and L. A. Baker, Chem. Commun. **2009**, 4877; S. Liu, Y. Yan, Y. Wang, S. Senapati, and H.-C. Chang, Biomicrofluidics **7**, 061102 (2013).
[12]J. Sherwood, M. Mao, and S. Ghosal, Langmuir **30**, 9261 (2014).
[13]J. Cervera, B. Schiedt, R. Neumann, S. Mafe, and P. Ramirez, J. Chem. Phys. **124**, 104706 (2006); J. Cervera, A. Alcaraz, B. Schiedt, R. Neumann, and P. Ramirez, J. Phys. Chem. C **111**, 12265 (2007).
[14]F. B. Hildebrand, *Advanced Calculus for Applications* (Prentice-Hall, 1976); A. Varma and M. Morbidelli, *Mathematical Methods in Chemical Engineering* (Oxford University Press, 1997).
[15]V. V. Nikonenko and A. E. Kozmai, Electrochim. Acta **56**, 1262 (2011).
[16]J. Hall, J. Gen. Physiol. **66**, 531 (1975); I. Vlassiouk, S. Smirnov, and Z. Siwy, Nano Lett. **8**, 1978 (2008).